Desalination and Water Treatment
www.deswater.com

doi: 10.5004/dwt.2017.20153

67 (2017) 28–40
March

Experimental and CFD investigation of a multistage centrifugal pump including leakages and balance holes

Osman Babayigit[a], Muammer Ozgoren[b,*], Muharrem Hilmi Aksoy[b], Osman Kocaaslan[c]

[a]*Selcuk University Hadim Vocational School, Konya, Turkey, email: obabayigit@selcuk.edu.tr*
[b]*Selcuk University, Mechanical Engineering Department, Konya, Turkey, emails: mozgoren@gmail.com (M. Ozgoren), muharremaksoy@selcuk.edu.tr (M.H. Aksoy)*
[c]*Selcuk University Huglu Vocational School Konya, Turkey, email: okocoaaslan@selcuk.edu.tr*

Received 1 March 2016; Accepted 13 August 2016

ABSTRACT

The aim of this study is to analyze numerically a multistage pump with some new approaches and compare the results with experimental data. A centrifugal pump, consisting of six backward curved blades, ten vane diffusers and two stages, was used. First, models of an impeller, a diffuser, suction and discharge sections of the centrifugal pump were separately designed by empirical equations. The flow volume of the pump was numerically solved by different turbulence models. Thus, the most accurate results in comparison with experimental data were obtained for the realizable k-ε turbulence model. For the purposes of this study, the effect of balance holes and leakages (clearances) on the performance was scrutinized. In most studies, it is not taken into consideration in computational fluid dynamics (CFD) analyses due to the difficulty of meshing these regions. The experimental studies were performed at a computer controlled pump test rig that was established according to the standard TS EN ISO 9906. The results of CFD/experimental analyses for the pump head, hydraulic efficiency and hydraulic power on the design point, having the flow rate of 80 m^3/h and the revolution of 2,975 rpm, were found to be 81.47/80.70 m, 51.98%/51.42% and 17.94/17.77 kW, respectively. The obtained CFD and experimental results were found to be close agreement for the design flow rate as well as for all tested flow rates. Other characteristics of the pump such as velocity, static pressure, streamline patterns and turbulence kinetic energy were also investigated. In addition, the leakages and balance holes have significantly affected the pump characteristics, which must be considered in CFD analyses in order to find more precise results for true-to-life simulations.

Keywords: Balance hole; CFD; Clearance; Hydraulic efficiency; Leakages; Multistage centrifugal pump

1. Introduction

Centrifugal pumps are widely used for the purpose of water supply, industrial applications, waste pump, water treatment, irrigation systems and much more [1,2]. In order to decrease the present 20% electricity consumption ratio of the pumps in the world, even a small improvement of efficiency of pumps enable to save a significant amount of energy [3,4]. Therefore, detailed analyses should be carried out on pumps including all physical, geometrical and material variables.

The number of blades is one of the design parameters and is determined depending on the other parameters. There are many pumps impeller, which have different number of blades in the industry. Especially on the radial flow pumps, most of the impellers have six blades. In addition, radial flow pumps are one of the commonly used types in the industry. So that six-blade numbers were used in this study owing to the providing satisfactorily necessary head and volume flow rate.

In recent years, with the rapid development of the computer technology and computational fluid dynamics (CFD), a numerical simulation has become an important tool to study detailed flow field in pumps and also to predict pump

* Corresponding author.

performance. CFD provides a cost-effective and accurate alternative to scale model testing with variations on the simulation being performed quickly [5–7]. Development in CFD makes available to analyze detailed flow structures in pumps [8].

A centrifugal pump consists of a set of rotation vanes enclosed within housing or casing that is used to impart energy to a fluid through centrifugal force [9]. There are several parameters that affect the pump efficiency and lifetime. The life and size of the bearings in centrifugal pumps are greatly influenced by the axial thrust generated by fluid flow. High axial thrust loads can cause rapid thrust bearing wear and either subsequent pump failure or frequent overhauls [10]. This axial force increases with the increasing stage number in multistage pumps. The impeller must be axially balanced if it is not possible to absorb the entire axial thrust in the axial bearing. There are several methods to reduce the thrust on the shaft but they result in hydraulic losses. One of the ways to balance this axial thrust is using balance holes. Balance holes in the impeller of the centrifugal pumps are mainly drilled into the hub surface. The balance holes connect the back of the impeller with the inlet area, where pressure is low. The leak flow through the holes influences the flow in the cavities above the impeller and thereby reduces the axial force but it results in leakage and reduces the pump efficiency [11].

There are also some other losses on the pump that should be considered. Some liquid is passed through the gap between rotor and stator in order to remove the heat created by the motor losses and fluid friction. To let the impeller rotate freely within the pump casing, small clearances should be designed between the impeller and pump casing. Therefore, a leak flow will occur in the gap between the rotating impeller and stationary pump housing. The rate of leak flow depends mainly on the design of the gap, the impeller pressure rise and impeller rotating speed. Clearances and balance hole causing leak flows are shown in Fig. 1. To minimize the amount of leak fluid through these clearances to increase the efficiency of the centrifugal pumps, some wearing ring or impeller seal can be used [12]. However, these precautions do not prevent these leakages completely.

Especially in the regions of leakages, it has been extremely challenging to create grids and analyses for simulation due to the very small size of the flow volume. Therefore, in many CFD studies, the effect of leakages and balance holes in a multistage centrifugal pump has not been investigated. This approach causes a deviation between the experimental and numerical results. Complicated leak flows, clearances and any balance holes make the hydrodynamic analyses very challenging without performing three-dimensional CFD analyses.

There are many studies related to the pump performance improvement in the literature. Some of them focuses on the detailed investigation of geometrical modifications and elaborates experimental tests. Three-dimensional turbulence flow simulation for centrifugal impellers was performed numerically in many studies [13–19]. In most of these studies, balance holes and leak flows are not considered.

There are few studies that express the importance of the clearances and effect of balance holes. Jiang et al. [20] carried out a numerical investigation of influence of the clocking effect on the unsteady pressure fluctuation and radial forces

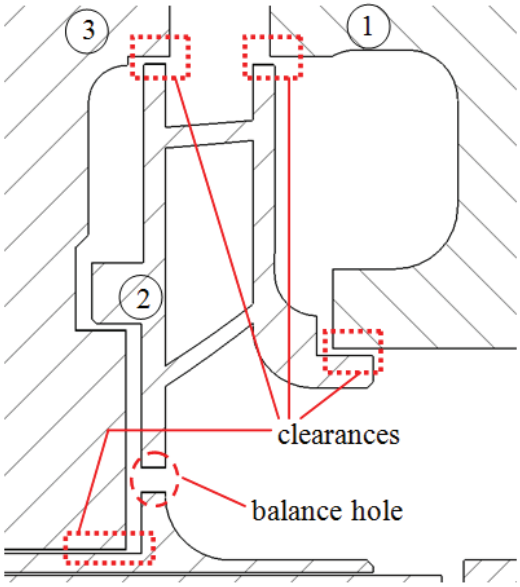

Fig. 1. Clearances and balance hole on a partial cross section view at one stage of the pump.

in the centrifugal pump. Numerical simulation based on the Reynolds-averaged Navier–Stokes (RANS) combined with the Shear Stress Transport (SST) k-ω turbulence model was used to obtain hydrodynamic performance of the centrifugal pump. The numerical results of the hydrodynamic performance have coincided with the experimental data. It was also proven that above or below the design flow rate the reason of the errors between experimental and numerical results in pump may occur due to neglecting of leakage loss through balancing holes. It was pointed out that the impact of balance holes and leakages cannot be neglected. Stel et al. [21] carried out a numerical study on the flow in a multistage, mixed-type electric submersible pump. They used a CFD program based on the finite volume method to find the numerical solution of the flow inside a multistage pump. It was concluded that the results provided by the numerical model are accurate enough and acceptable for the purposes of the study. They inferred that some differences in numerical and experimental study due to the leakage flows and gaps were not considered. The study about the impact of centrifugal pump side clearance on pump performance was carried out numerically by Ayad et al. [22]. The influence of the variation of the centrifugal pump side clearance width (0:0.2 impeller width) on the centrifugal pump performance parameters at different flow rates (0:5 L/s) was investigated. It was proven that the impeller side clearance had a great regression effect on the centrifugal pump performance. Engeda and Rautenburg [23] performed a systematic study on semi-open impellers and yielded a conclusion that the tip clearance had an evident effect on pump performance. Liu et al. [24] conducted experimental and numerical investigations for tip clearance effect on impeller-geometry of mini turbo-pump. In the performance tests, rotational speed varied between 3,000 and 10,000 rpm, and the axial clearance at the blade tip of

impeller exit was between 0.2 and 0.8 mm. They came to the conclusion that the clearance has affected the pump performance significantly and its effect could be attenuated by the impeller geometry such as larger outlet blade angle.

Although some studies are done on the analyses of centrifugal pumps as aforementioned above, a study on a two-stage centrifugal pump performance including the effect of leakage flow losses and balance holes has not been encountered. The motivation of this paper is to perform both numerical and experimental studies on a multistage centrifugal pump in order to provide the lacking data. Moreover, the effect on the flow structure of the leakage losses and the balance holes was examined in detail.

2. Material and methods

In this study, a volume flow rate, head and revolution values of a two-stage centrifugal pump with a vertical shaft were selected. The impeller, a diffuser, suction and discharge sections of the centrifugal pump were separately designed using the empirical equations and were drawn using ANSYS-BladeGen and Solidworks software [12]. Then, the numerical analyses of the designed pump were made in ANSYS-Fluent software to determine the optimum geometry of impeller and diffuser to be manufactured. Finally, performance test of the manufactured pump was performed to compare the numerical results with experimental ones.

2.1. Numerical study

ANSYS-Fluent program for the numerical analyses of the selected pump operations were performed in the following order:

- designing and drawing of the pump impeller, the diffuser, the suction and the discharge sections;
- creating the flow volume and mesh structure;
- performing the CFD analyses under proper boundary conditions; and
- obtaining the pump flow characteristics as head, hydraulic power and hydraulic efficiency.

The main design parameters and geometric specification of the examined pump are given in Tables 1 and 2. The cross sections of the impeller and the diffuser are presented in Figs. 2 and 3.

2.1.1. The solid model and flow volume of the pump

First, models of the diffuser, the suction and discharge sections of the pump are separately designed using Solidworks software as shown in Fig. 4(a). After designing of the pump sections, a solid model of the pump was completed, and flow volume at inlet, within the pump, and outlet were formed by closing the suction and discharge region of the pump as it can be seen in Fig. 4(b).

2.1.2. Creating mesh structure

CFD studies are performed in seven different grid sizes for the grid independency test to diminish the influence of the number of grids/grid size on the computational results as shown in Fig. 5. As the mesh size increases up to 38 million, the hydraulic efficiency and pump head reach to asymptotic value at 25×10^6 and became independent of the mesh size and a mesh number. Therefore, this mesh size was applied to all analyses to save the computation time. A relativity examination of the grid number was done to obtain grid independency. The effect of grid number on pump characteristics less than 1% is acceptable [25].

The occurrence of leak flow regions has 0.3 mm gap width. It is observed a decrease in mesh quality when mesh transition from large surfaces to very small leakage surfaces has been realized. Therefore, in this study before forming mesh structure, flow volumes of leakages are separately defined and meshed as shown in Fig. 6. In addition, eight layers of the inflation were used for the impeller volume by creating thin elements that can correctly capture the velocity and pressure gradients near the no-slip walls. The flow domain of the diffuser, the impeller, suction and the discharge section of the pump volume were meshed with tetrahedral cells, and small leakage flow regions of the pump volume were meshed with hexagonal cells as it is shown in Fig. 6. Hexagonal mesh increases the mesh quality especially in small volumes and

Table 1
Specifications of the multistage pump

Description	Parameter	Value
Design flow rate (m^3/h)	Q_d	80
Single-stage head (m)	h_s	40
Rotating speed (rpm)	n	2,975
Stage number	N	2
Specific speed	n_q	28

Table 2
Geometric parameters of the impeller and diffuser

Description	Parameter	Value
Impeller		
Inlet diameter (mm)	D_1	100
Inlet blade angle (°)	β_1	27
Inlet blade width (mm)	b_1	23
Outlet diameter (mm)	D_2	205
Outlet blade angle (°)	β_2	20
Outlet blade width (mm)	b_2	14
Blade wrap angle (°)	φ	125
Blade number	z	6
Diffuser		
Inlet diameter (mm)	D_3	206
Inlet blade angle (°)	β_3	9
Vane number	z_v	10
Outlet diameter (mm)	D_4	274
Return vane number	z_r	8
Vane wrap angle (°)	φ_v	50
Return vane wrap angle (°)	φ_r	25

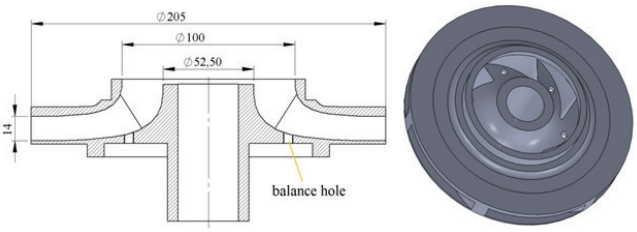

Fig. 2. Cross section view and solid model of the impeller.

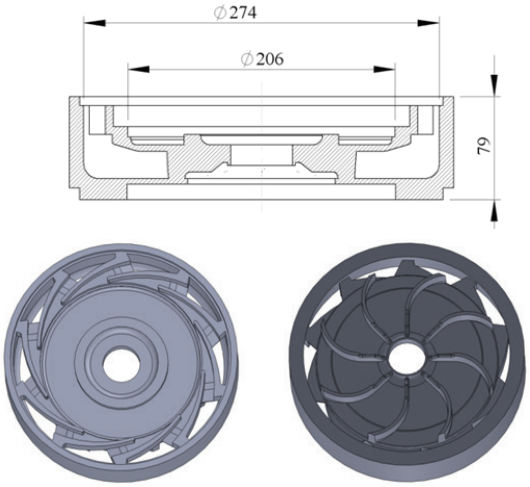

Fig. 3. Cross section view and solid models of the diffuser.

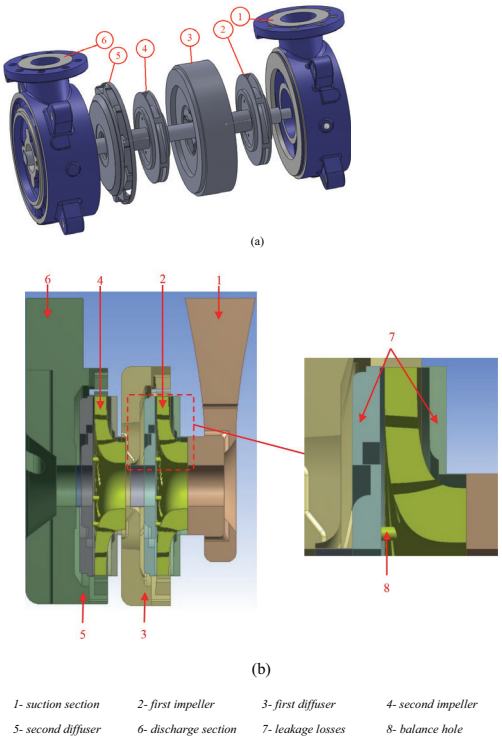

Fig. 4. Pump appearance: (a) demounted solid model and (b) flow volume of the pump.

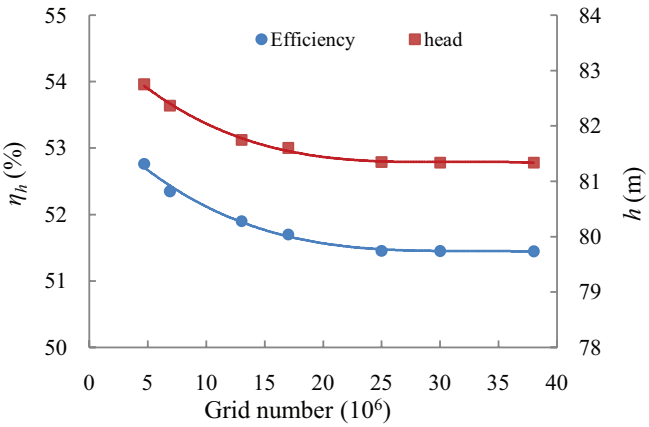

Fig. 5. Performance characteristics of the pump for different grid numbers.

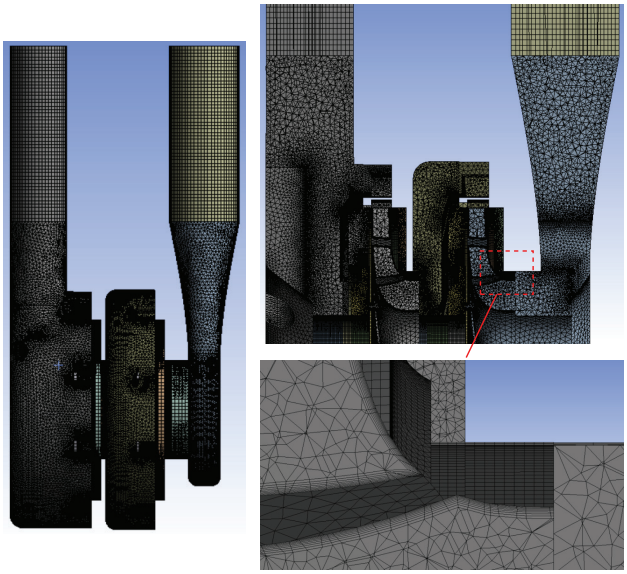

Fig. 6. Mesh structures of the fluid domain of the pump.

decreases the number of grids but it is not possible to apply it to complex geometries such as an impeller and a diffuser. Average and minimum orthogonal values of the mesh quality were found to be 0.85 and 0.15, respectively.

2.1.3. Numerical analysis

To represent the flow phenomena of the pump, some of the common methods for the steady analyses in the literature SST k-ω, standard k-ε and realizable k-ε turbulence models were examined; thus, realizable k-ε turbulence model was found to be appropriate for CFD analysis of the present centrifugal pump. The boundary conditions were taken for the real operation conditions as given in Table 3. The realizable k-ε turbulence model and SIMPLEC algorithm were applied to solve the equations. The simulation was assumed

Table 3
Boundary conditions for the present study

Position	Boundary condition
Inlet	Mass flow inlet
Outlet	Pressure outlet
Walls at hub and shroud	Non-slip wall
Impeller	Rotating reference frame
Interface	General connection
Wall function	Standard wall function

to be steady flow, and moving reference frame was applied to the impeller-diffuser interaction surfaces. Mass flow rate was specified in the pump inlet, and static pressure was used at the pump outlet. Average height of surface roughness was measured to be approximately 0.035 mm for all non-machined surfaces as the property of the sand casting production with the sanding process and structure properties of the cast iron material. Non-slip wall conditions were applied on all the physical surfaces except the interfaces between different parts of the flow surfaces of the multistage blades and diffuser connections. Residuals of the numerical calculation were set to 10^{-5} for the static pressure value at the pump outlet. When the overall imbalance of the calculated parameters was less than 0.1% or the minimum residual was reached, the simulation was assumed to be converged for final computation. If the value of y^+ is found to be between 30 and 100, it shows the results of the grid structure can be acceptable [26]. In this study, the overall value of y^+ was found to be between 30 and 80.

The ANSYS FLUENT software was used to solve including the centrifugal force source in the impeller and the steady terms. Turbulent flow in the pump was simulated using the realizable k-ε model. For three-dimensional incompressible, steady flow, the continuity and momentum equations are written as follows [27–29]:

$$\nabla\vec{V} = 0 \tag{1}$$

$$\rho\nabla(\vec{V}\vec{V}) = -\nabla P + \mu\nabla^2\vec{V} + \vec{\rho g} + \vec{F} \tag{2}$$

Transport equations for the realizable k-ε model are as follows:

$$\frac{\partial}{\partial x_i}(\rho K u_j) = \frac{\partial}{\partial x_i}\left[\left(\mu + \frac{\mu_t}{\sigma_k}\right)\frac{\partial k}{\partial x_j}\right] + G_k + G_b - \rho\varepsilon - Y_M + S_k \tag{3}$$

$$\frac{\partial}{\partial x_i}(\rho\varepsilon u_j) = \frac{\partial}{\partial x_i}\left[\left(\mu + \frac{\mu_t}{\sigma_\varepsilon}\right)\frac{\partial \varepsilon}{\partial x_j}\right] + \rho C_1 S\varepsilon - \rho C_2 \frac{\varepsilon^2}{k + \sqrt{v\varepsilon}} + C_1\varepsilon\frac{\varepsilon}{k}C_3 G_b + S_\varepsilon \tag{4}$$

where:

$$C_1 = \max\left[0.43\frac{\eta}{\eta + 5}\right] \tag{5}$$

$$\eta = S\frac{k}{\varepsilon} \tag{6}$$

$$S = \sqrt{2S_{ij}S_{ij}} \tag{7}$$

In the given equations, $G_{k\varepsilon}$ represents the generation of turbulence kinetic energy due to the mean velocity gradients; G_b is the generation of turbulence kinetic energy due to buoyancy; Y_M represents the contribution of the fluctuating dilatation incompressible turbulence to the overall dissipation rate; C_2 and $C_{1\varepsilon}$ are constants and σ_k and σ_ε are the turbulent Prandtl numbers for k and ε, respectively. S_k and S_ε are user-defined source terms [30]. The standard values of different constants appearing in equations ($C_{1\varepsilon} = 1.44$, $C_2 = 1.9$, $\sigma_k = 1.0$, $\sigma_\varepsilon = 1.2$) were used in the present computations [31]. The solution of Eqs. (3) and (4) gives spatial variation of k and ε, which, in turn, can be used to find out spatial variation of turbulent viscosity or eddy viscosity μ_t using the Prandtl–Kolmogorov relation [28,32]:

$$\mu_t = \rho c_\mu \frac{k^2}{\varepsilon} \tag{8}$$

After performed the numerical analysis, hydraulic efficiency of the pump was calculated using pump head in m unit (h), volume flow rate in m^3/s ($\dot{Q}$), angular velocity in rad/s (ω), revolution in rpm ($\dot{n}$) and torque value in Joule (T) as follows [33]:

$$P_h = \frac{\rho g \dot{Q} h}{1000} \tag{9}$$

$$P_s = \frac{T\omega}{1000} \tag{10}$$

$$\omega = \frac{\pi\dot{n}}{30} \tag{11}$$

$$\eta_h = \frac{P_h}{P_s} \tag{12}$$

2.2. Experimental setup

The elements of the set up are as follows:

- a differential pressure transmitter, which was located between the pump inlet and outlet,
- a magnetic flow meter, which was used for measuring the flow rate by a throttle valve to regulate it manually, and
- an electrical control panel to measure values of voltage and current.

Experimental setup is schematically depicted in Fig. 7. The experiment was repeated for the different flow rates by adjusting the throttle valve at the revolution of 2,975 rpm. The values measured by the volume flow meter, differential pressure transmitter and electrical control panel were recorded and processed.

Hydraulic power and hydraulic efficiency were calculated using the experimental data from the Eqs. (9) and (12) while Eqs. (13) and (14) were used to calculate electrical and shaft power, respectively.

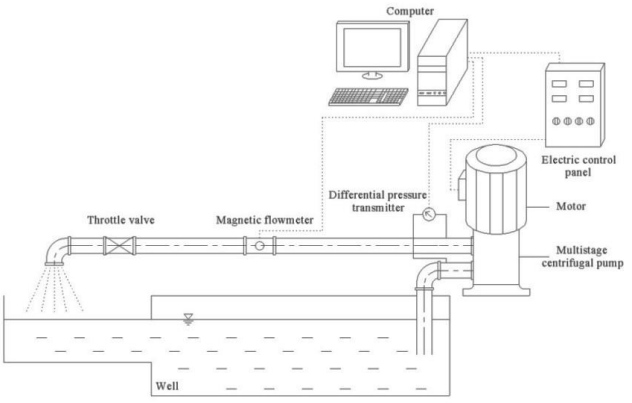

Fig. 7. Schematic view of the test rig.

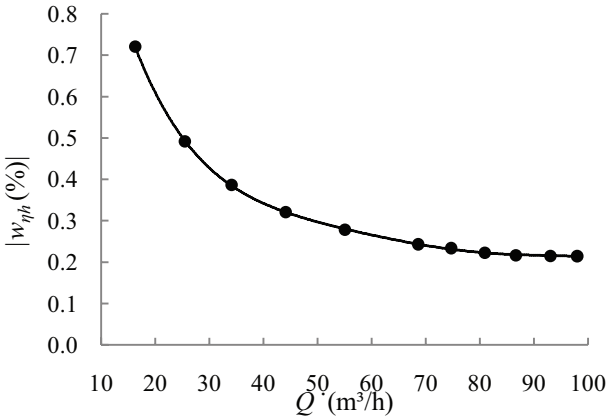

Fig. 8. Variation of uncertainty against volume flow rate.

$$P_e = \frac{\sqrt{3} I \cos\varphi V}{1000} \tag{13}$$

$$P_s = P_e \eta_e \eta_m \tag{14}$$

The efficiency of the electric motor and all mechanic loses were taken from the manufacturer of the motor according to loading percentage and also taken into account in experiments. In the experimental studies, uncertainties occurred because of measuring equipment, the surrounding environment and human errors made by the person doing the experiment. In each experiment, the efficiency uncertainty, $w_{\eta h}$, caused by different independent variables can be expressed as in Eq. (15) [34,35]. The uncertainty values were calculated with respect to the specifying effects of total errors for the measured quantities, achieving more accurate measurements and assisting in reducing the uncertainties.

$$w_{\eta_h} = \pm \frac{\left[\left(\frac{\partial \eta_h}{\partial P}\omega_P\right)^2 + \left(\frac{\partial \eta_h}{\partial \dot{Q}}\omega_{\dot{Q}}\right)^2 + \left(\frac{\partial \eta_h}{\partial I}\omega_I\right)^2 + \left(\frac{\partial \eta_h}{\partial V}\omega_V\right)^2 + \left(\frac{\partial \eta_h}{\partial \varphi}\omega_\varphi\right)^2\right]^{\frac{1}{2}}}{\eta_h} 100 \tag{15}$$

Here, η_h presents the calculated hydraulic efficiency using Eqs. (9)–(14). Variables $w_{\dot{Q}}$, w_P, w_I and w_V show, respectively, accuracy values of the measurement devices for volume flow rate, differential pressure transmitter, ampere meter and voltmeter while $w_{\eta h}$ is relative uncertainty amount (±%) of dependent variable efficiency for the calculation derived from the measured and taken values. Accuracy values of the measurement parameters for pressure transmitter (Pa), flow rate (m³/h), electric current (*A*), voltage (*V*) and cosφ value were taken as ±0.05%, ±0.04%, ±0.1%, ±0.1% and ±0.1%, in sequence.

Other parameters in Eqs. (9)–(14) were assumed to be constant. Variation of relative uncertainty against the volume flow rate is given in Fig. 8. Uncertainty values of the efficiency in Eq. (12) depending on the measurement devices and parameters such as pump inlet and outlet pressures, volume flow rate, water density, electric current, voltage and electric motor efficiency were found to be less than ±1%. Continuing decreasing of uncertainty values occurs due to the fact that volume flow rate increment is more dominant on the calculation of hydraulic efficiency than the other measurement parameters including even high magnitudes of the pressure difference between the inlet and outlet of the pump.

3. Results and discussion

In this study, a multistage centrifugal pump was experimentally and numerically examined. Parameters chosen according to the industrial application were $\dot{Q}$ = 80 m³/h, $\dot{n}$ = 2,975 rpm and h = 80 m, which were provided by Sempa Pump Company in Turkey. These parameters were used as initial values for CFD analysis. For CFD analysis of the pump performance, revolution was kept constant while the volume flow rate was changed from 16 to 98 m³/h. After the iterations converged, the parameters of mass flow rate, turbulence kinetic energy, turbulence distribution rate and velocity values were controlled to check if the convergence is in the range of acceptable level of 10^{-5}.

In flow analysis for the design flow rate, SST k-ω, standard k-ε and realizable k-ε turbulence models were applied, and the results were presented in Table 4. The realizable k-ε turbulence model has given the best result when compared with the obtained experimental data. The results of CFD/experimental analysis for the pump head and hydraulic efficiency at the design flow rate of 80 m³/h were found to be 81.47/80.70 m and 51.98%/51.42%, respectively.

According to the CFD results, the maximum hydraulic efficiency and the head values were calculated as 51.98% and 81.47 m, respectively. A comparison of the hydraulic efficiency and head value with the volume flow rate for the experimental and numerical results of the pump systems is presented in Figs. 9(a) and (b). The hydraulic efficiency is increasing with increasing volume flow rate up to 80 m³/h for the experimental and CFD results while decreasing head occurs at the exit of the pump as expected for the general pump characteristics curve. The difference between the experimental and numerical simulation results is decreasing as the flow rate approaches to the design point value of 80 m³/h, and then, it is increasing with higher flow rate and decreasing in the head due to the complex flow physics.

Comparison of numerical and experimental hydraulic power vs. the flow rate is demonstrated in Fig. 9(c). The hydraulic moment increases until the best efficient point value of 80 m³/h is reached, and then, it decreases slightly because of having more effective head decrement than volume flow rate increment as commented in Eq. (9). Variation of relative difference between the CFD and experimental results is shown in Fig. 9(d). It is seen that relative difference is the smallest for the best efficiency point, and it increases with increasing or decreasing volume flow rate values. That is, the relative differences were found to be in the range of 1%–10% while it was only 1% at the best efficient point. Furthermore, the deviation between the experimental and CFD results for head, hydraulic efficiency and hydraulic power values were found to be in the range of less than 10% for all flow volume rates and those values were, respectively, determined as 0.95%, 1.1%, and 0.96% at design flow volume rate. Provided results demonstrate that the applied CFD simulations enable to predict the pump performance within an acceptable accuracy [26,36].

Table 4
Comparison of numerical results with different turbulence models on design flow rate

Model	Head (m)	Hydraulic efficiency (%)
k-ω SST	77.64	50.74
k-ε standard	79.83	50.35
k-ε realizable	81.47	51.98
Experimental data	80.70	51.42

The pumps are designed according to head, flow rate and revolution values. Depending on the distance to the design flow rate by varying pressure and the velocity of fluid in the pump may occur some disorders such as: flow separations, reverse flows, circulating flows and cavitation. Hence, the turbulence effects on the off-design flow rates are increased. The accuracy of the results, obtained by the turbulence model used in CFD, depends on its representation ratio of the occurred turbulence effect. Therefore, the relative differences between the experimental and CFD values are higher at off-design flow rates as seen in Fig. 9.

Numerical flow visualization studies on a separate plane formed on the pump flow rate were conducted. The YZ plane was generated from the center of a balance hole of the pump flow volume. The cross-sectional view of the flow volume on this plane is shown in Fig. 10. The flow characteristics such

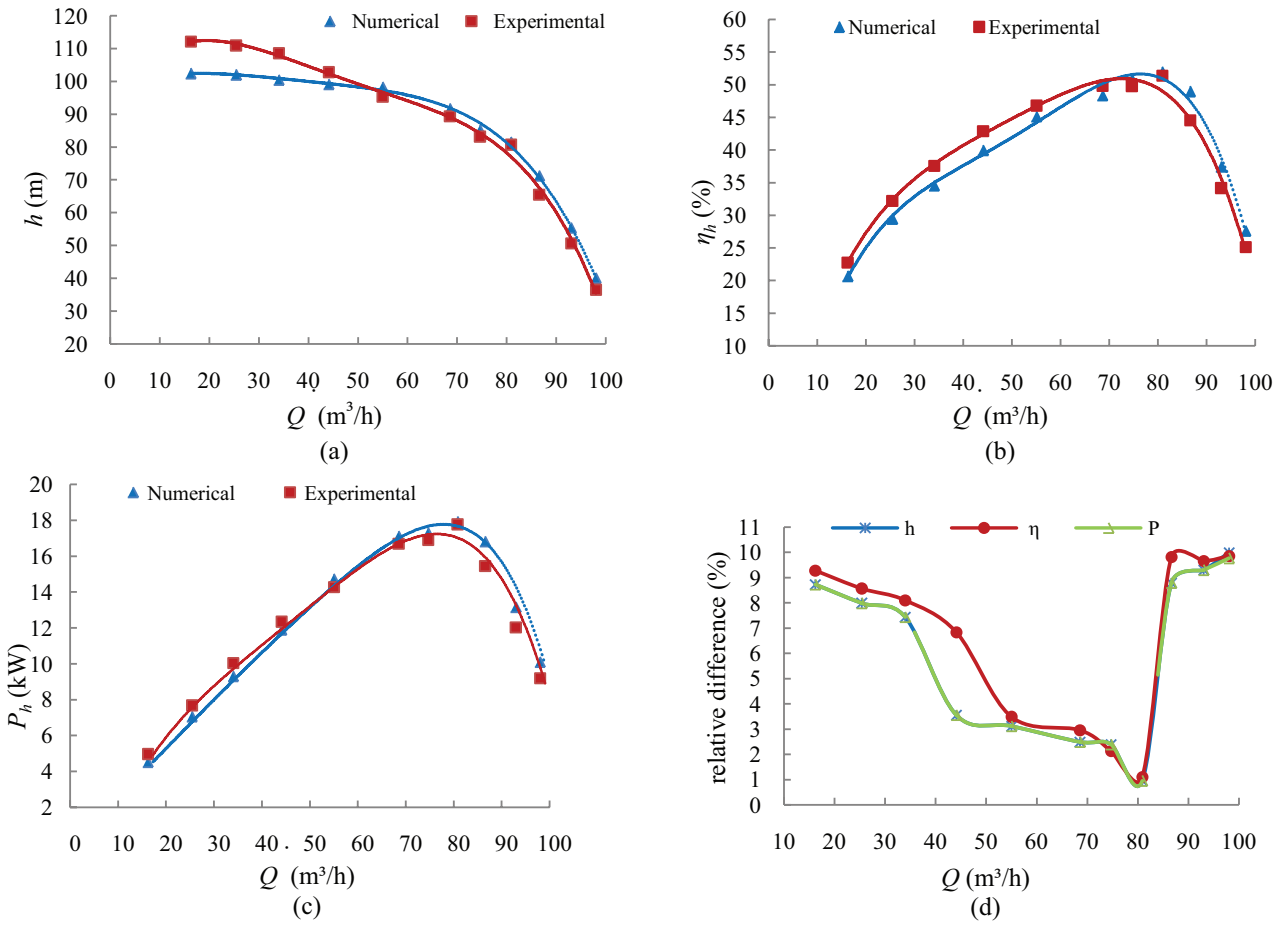

Fig. 9. Comparison of the numerical and experimental: (a) head, (b) hydraulic efficiency, (c) hydraulic power of the pump vs. the volume flow rate and (d) the variation of relative difference between the CFD and experimental results.

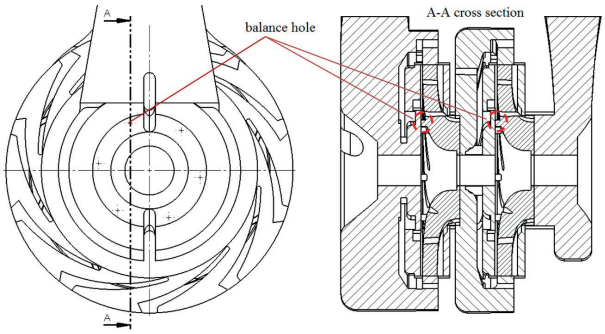

Fig. 10. CFD flow visualization plane on YZ.

as velocity vectors, velocity contours, streamline patterns and static pressure for the flow rates of 55, 80 and 93 m³/h for the impeller models with and without balance holes are prepared at this plane as shown in Figs. 11–13.

Two-dimensional vector fields and corresponding velocity contours in YZ cross-section plane are indicated in Fig. 11, in which acceleration and deceleration of the flow ways can be seen clearly. From the exit of the impeller to the entrance of the diffuser, flow becomes slower due to the increasing flow area. The reverse flows and increasing of flow velocity in the region, where the clearances and balance holes were formed, can be seen in Figs. 11 and 12. When the impeller model without balance holes compared with the balance holes in all three flow rates; lower velocity values were seen at the leakage flow region in front of the impellers; on the other hand, a quite low velocity occurred at the leak flow region behind impellers. It is seen in Fig. 11 that the velocity is getting lower by the decreasing flow rate in the pump inlet region. A swirling flow occurs due to the large velocity gradient, and thus, focus forms around tip of the blade as seen from streamline topology in Fig. 12. A slight increase for the flow velocity and reverse flow in the entrance region of the discharge section was also noticed. Curved and recirculated streamline patterns demonstrate the acceleration, deceleration and flow separation phenomena.

Fig. 13 displays the static pressure contours at the same plane in Figs. 11 and 12. As it can be seen from the all colored legends, the static pressure increases gradually from the pump suction to the discharge side. In the absence of balance holes, higher static pressure distributions were occurred toward the pump outlet compared with the ones with balance holes in all three flow rates. In addition, when flow rate increase, a remarkable drop in static pressure was obtained from the second stage to the pump outlet for all three flow rates with and without balance holes.

The effects of balance holes on the axial force on the pump are also investigated. All forces in the axial direction are measured and compared at the design flow rate of 80 m³/h for the impeller models with and without balance holes. The CFD analyses show that the magnitude of the total axial forces was found to be 875 N without balance holes; whereas, it was reduced up to 3 N when balance holes are applied. It can be concluded that the balance holes have the great effect on reducing the total axial forces.

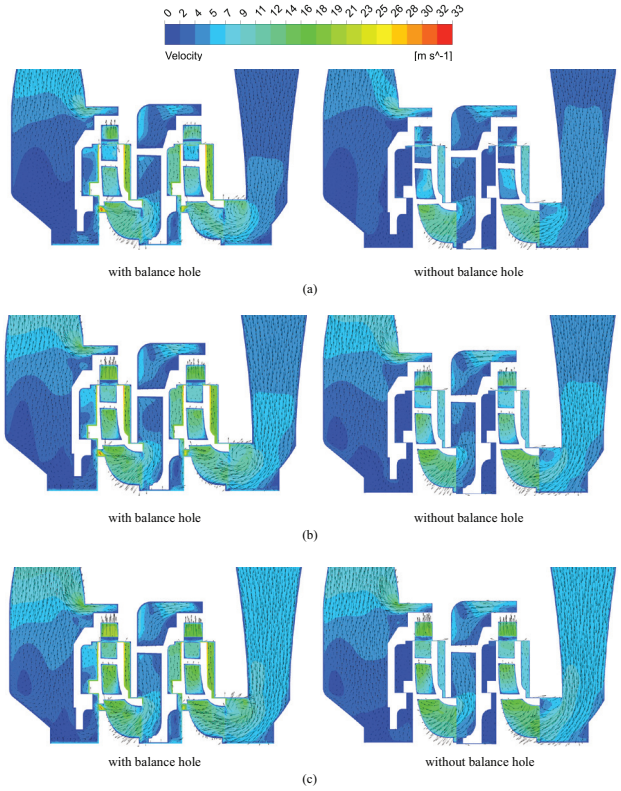

Fig. 11. Tangential velocity vector and contours on YZ plane on flow rates of: (a) 55 m³/h, (b) 80 m³/h and (c) 93 m³/h.

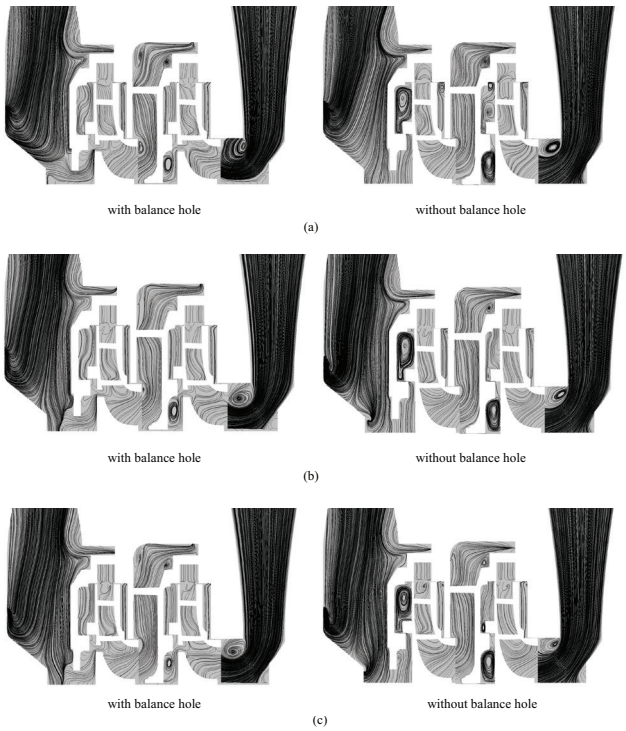

Fig. 12. Streamline patterns on YZ plane on flow rates of: (a) 55 m³/h, (b) 80 m³/h and (c) 93 m³/h.

Fig. 13. Static pressure contours on YZ plane on flow rates of: (a) 55 m³/h, (b) 80 m³/h and (c) 93 m³/h.

All leakages passing through the balance holes and clearances between the impeller, the diffuser and suction side are shown in Fig. 14. The total leak flow is determined as follows:

$$\dot{Q}_L = \dot{Q}_{L1} + \dot{Q}_{L2} + \dot{Q}_{L3} \tag{16}$$

Here, $\dot{Q}_{L1}$ is the leakage occurring from outlet to the inlet side of the impeller, and it is included to the main flow entering into the inside of the impeller. $\dot{Q}_{L2}$ is the leakage existing from outlet to the back size of the impeller. $\dot{Q}_{L3}$ is the leakage happening from diffuser outlet to the back size of the impeller in a similar manner, and $\dot{Q}_L$ represents the total leakages. Both $\dot{Q}_{L2}$ and $\dot{Q}_{L3}$ are back into the impeller inside from balance holes located at the rear side of the impeller. It is evident that all the leakage stream flow toward the low-pressure region from the high-pressure side is shown in Figs. 13(b) and 14.

Variation of the total leakages and the ratio of leak flows against the main flow is shown in Fig. 15. As seen, the total leak flow is almost unchanged at all main flow rates. However, it is observed that the ratio of the total leak flow rate is increasing with the decrease of the main flow rate in a significant way. This ratio is about 9% at the design flow rate while rising up to about 50% at low flow rates. Leak flow mainly depends on the clearance geometry, impeller rotational speed and head [37,38]. In case of fixed geometrical features and constant rotating speed as this study, leak flows therefore depend on the impeller static pressure mainly. The static pressures at the exit of the first impeller were nearly the same in different flow rates as seen in Fig. 13. Therefore, leak flow rates were found to be close to each other.

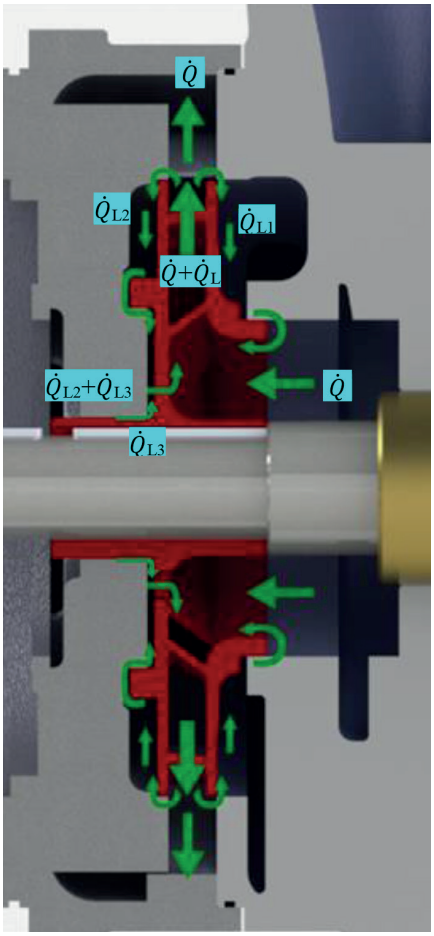

Fig. 14. Representation of the flow directions in the first stage of the pump.

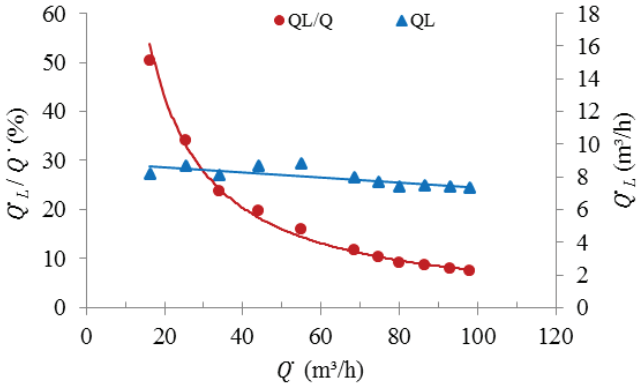

Fig. 15. Variations of the total leakages and the ratio of leak flows depending on the flow rate.

All leakage flow rates detected for design flow rate of 80 m³/h are given in Table 5. It is seen from the table that $\dot{Q}_{L1}$, $\dot{Q}_{L2}$ and $\dot{Q}_{L3}$ are approximately 41%, 42% and 17% of the total

Table 5
Main and leakage flow rates on the design point

Parameter	Volume flow rate (m^3/h)
$\dot{Q}$	80
$\dot{Q}_L$	7.38
$\dot{Q}_{L1}$	3.05
$\dot{Q}_{L2}$	3.06
$\dot{Q}_{L3}$	1.27

leak flow rate of $\dot{Q}_L$ = 7.38 m^3/h, respectively. These different ratios occur depending on the gap distance and the pressure difference.

The mid-span planes on XY plane were generated from the center of the impellers. A cross-sectional view of the flow volume of the pump on these planes is shown in Fig. 16. Tangential velocity vectors on the total velocity, static pressure contours and turbulence kinetic energy contours for the first and the second stages of the impeller models with and without balance holes on the mentioned planes are presented in Figs. 17 and 18. It can be interpreted from these images that the impeller and geometry design of diffuser convert smoothly the mechanical shaft power to the flow energy.

When the balance holes are included, flow separation, formed around positive pressure sides of the impeller blades, decreases. Velocity distribution around balance holes is higher than in the other regions for both stages as seen in Figs. 17(a) and 18(a).

As indicated in Figs. 17(b) and 18(b), in the absence of balance holes, regular increase of static pressure is seen from the entrance to the exit of the impeller for both stages. However, in the presence of balance holes, a sudden pressure drop through the six balance holes placed around the flow entrance region between the blades occurs due to the large pressure difference between the stages. Increments of the static pressure for both stages are approximately the same when the momentum effect is neglected because of the balance hole.

The turbulence kinetic energy dissipation for both stages occurs in a similar manner as shown in Figs. 17(c) and 18(c). When there aren't any other balance holes, nearly the same turbulence kinetic energy distributions occur through the planes for both stages. It can be seen that the turbulence kinetic energy values increase in regions where the balancing holes and entrance of the diffuser vanes were located. The distinguished increment of the turbulence kinetic energy values takes place around the balance holes. Moreover, it is demonstrated that the effect of the balance holes causes the pressure magnitude decrement as presented in Figs. 17(b) and 18(b).

To show the effect of balance hole on the pump stage, some points are created crossing over the balance hole in mid-span on XY plane in the first and the second impellers as shown in Fig. 19. The point indicated by number 3 is located in the center of the balance hole. Static pressure and turbulence kinetic energy values on these points are measured for the impeller models with and without balance holes. It can be seen in the Fig. 20(a) that the static pressure of the impeller model without

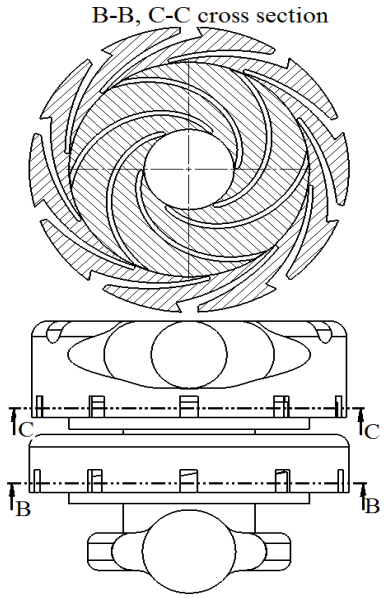

Fig. 16. CFD flow visualization mid-span planes on XY for the first and second stage.

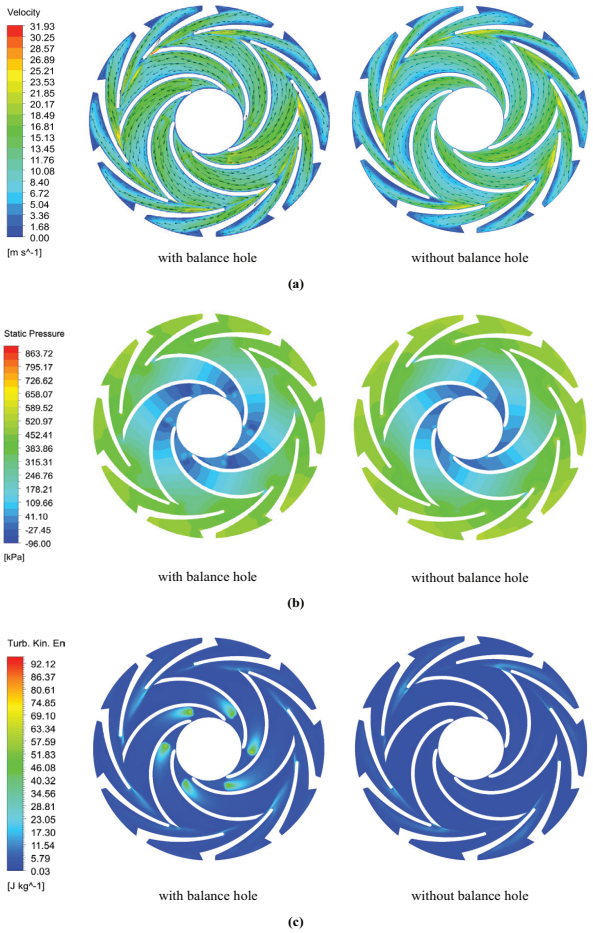

Fig. 17. (a) Tangential velocity vectors and contours, (b) static pressure contours and (c) turbulence kinetic energy contours at mid-span on XY for the first stage on the design flow rate.

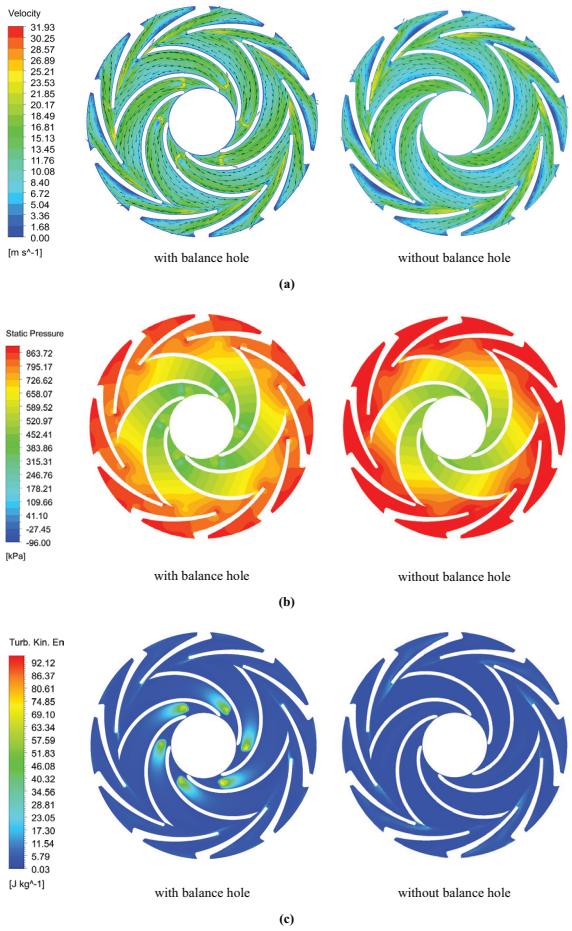

Fig. 18. (a) Tangential velocity vectors and contours, (b) static pressure contours and (c) turbulence kinetic energy contours at mid-span on XY for the second stage on the design flow rate.

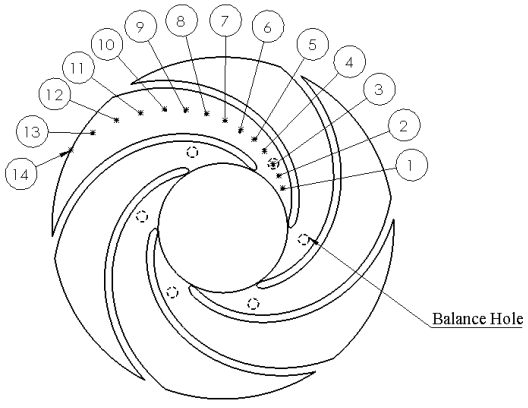

Fig. 19. The points following blade-profile and crossover balance hole at mid-span plane of the impeller.

balance holes continuously increases up to region close to the exit of the impeller. While approaching to the exit of the impeller, the static pressure increases at slower rate. In case of the impeller model with balance holes, static pressure increases on a regular basis from the impeller entrance to the balance hole, but it shows a sharp decrease on the balance hole, and then, it is

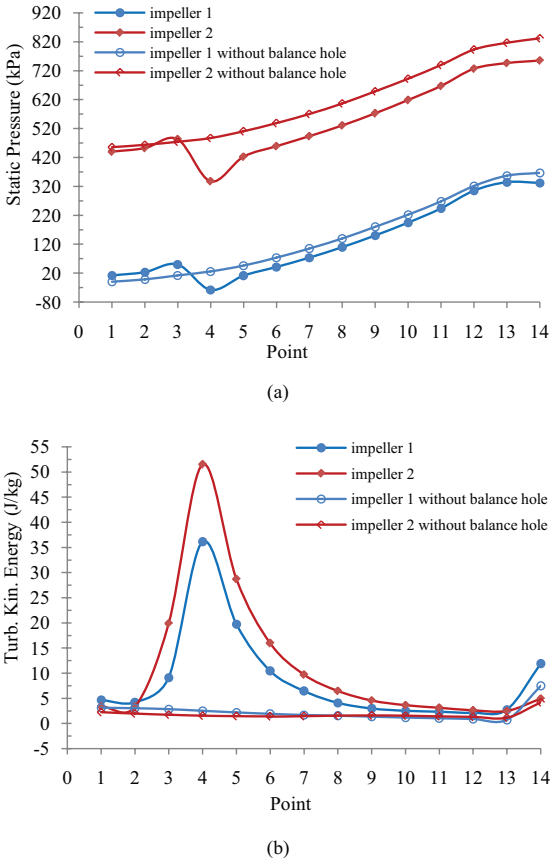

Fig. 20. (a) Static pressure and (b) turbulence kinetic energy on defined points shown in Fig. 19 for the first and second stage on design flow rate for the impeller models with and without balance holes.

linearly increasing again until reaching the impeller exit to the location point 12. The static pressure shows a small decrease on the impeller exit while increasing turbulence kinetic energy due to the mixing and sectional differences between the impeller exit and diffuser entrance.

It can be seen from the Fig. 20(b) that the turbulence kinetic energy of the impeller model without balance holes stays almost constant up to the impeller exit. While approaching the exit, the turbulence kinetic energy rises. While the impeller model with balance holes is taken into consideration, turbulence kinetic energy nearly does not change from the impeller entrance to the balance hole, but it increases significantly on the balance hole and takes its maximum value at point 4. Then it starts decreasing for a while and nearly stays unchanged to the impeller exit. It shows an increase on the impeller exit due to sectional differences between the impeller exit and diffuser entrance. It can be inferred that balance holes are the major factor, which causes turbulence kinetic energy in the impeller.

4. Conclusions

In this work, the CFD simulations and experimental studies of a two-stage centrifugal pump were presented in detail including the effects of balance holes and leakages.

The numerical results of the pump obtained by CFD were compared with the test results of the pump manufactured by Sempa Company in Turkey. The following improvements and achievements were obtained:

- The CFD analyses of the pump were completed under different operational conditions including the balance holes and the leakages providing a real case simulation. Thus, the experimental and numerical results were nearly overlapped with each other. The best results of the CFD and experimental analyses for the pump head, hydraulic efficiency and hydraulic power on the flow rate of 80 m^3/h were found to be 81.47/80.70 m, 51.98%/51.42%, and 17.94/17.77 kW, respectively.
- Variation of relative difference between the CFD and experimental results shows that the relative difference is the smallest for the best efficiency point and it increases with increasing or decreasing volume flow rate values. That is, the relative differences were found to be in the range of 1%–10% while it was only 1% at the best efficient point.
- It is also shown that the balance holes affect the flow structures, pressure distributions and turbulence kinetic energy values significantly so that it should be considered in CFD studies.
- Balance holes reduce the hydraulic efficiency of the pump by increasing the leak flow, although it is important to reduce the axial forces of the pump shaft. Designing double-suction pumps can be an alternative to balance these axial forces.
- It is revealed that the obtained experimental results are repeatable and reliable because of having very low uncertainty values around ±1%.
- It is demonstrated as seen in Table 5 that $\dot{Q}_{L1}$, $\dot{Q}_{L2}$ and $\dot{Q}_{L3}$ are approximately 41%, 42% and 17% of the total leak flow rate of $\dot{Q}_L$ = 7.38 m^3/h, respectively. These different ratios occur depending on the gap distance and the pressure difference. The ratio of the total leak flow to the design flow rate is around 9% for the examined pump.
- Parameters that determine the leak flow rate are the size of the clearances between the fixed and rotating components of the pump. It is not possible to prevent the leakage, but some solutions can be applied to reduce these clearances such as using seal and wear rings.
- Achieving an optimal balance between leakage and friction can be an essential goal for the future studies as small gap limits of the leakage flow; however, balance elements increases the friction, risk of drag and noise.
- In future, some studies on the location and a size optimization of the balance holes for the pump performance increment can be performed.

Acknowledgments

This work is supported by SANTEZ program of the Ministry of Science, Industry and Technology of Turkey with number 01076.STZ.2011-2 and Selcuk University's Scientific Research Project Office Contract No.: 14401075. The authors also would like to thank to the partner of the project Sempa Co. board (http://www.sempaltd.com/en/) for their support. This study is a part of Osman Babayigit's PhD Thesis.

Symbols

b_1 — Entry width of the impeller, mm
b_2 — Exit width of the impeller, mm
C_1 — k-ε model constant
C_2 — k-ε model constant
$C_{1\varepsilon}$ — k-ε model constant
$C_{2\varepsilon}$ — k-ε model constant
C_3 — k-ε model constant
C_μ — k-ε model constant
D_1 — Impeller inlet diameter, mm
D_2 — Impeller outlet diameter, mm
D_3 — Diffuser inlet diameter, mm
D_4 — Diffuser outlet diameter, mm
$\vec{F}$ — External body force
g — Acceleration of gravity, m/s^2
G_k — Generation of turbulence kinetic energy due to the mean velocity gradients
G_b — Generation of turbulence kinetic energy due to buoyancy
h — Pump head, m
I — Current, A
K — Turbulence kinetic energy, m^2/s^2
n_q — Specific speed
$\dot{n}$ — Rotating speed, rpm
N — Stage number
P — Static pressure, Pa
P_e — Electric power, kW
P_h — Hydraulic power, kW
P_s — Shaft power, kW
$\dot{Q}$ — Volume flow rate, m^3/h
$\dot{Q}_L$ — Total leak volume flow rate, m^3/h
$\dot{Q}_{L1}$ — Leak volume flow rate, m^3/h
$\dot{Q}_{L2}$ — Leak volume flow rate, m^3/h
$\dot{Q}_{L3}$ — Leak volume flow rate, m^3/h
S — Mean strain-rate of the flow
S_{ij} — Deformation tensor
S_k — User defined source term
S_ε — User defined source term
t — Time, s
T — Torque, N.m
u_j — y direction component of velocity vector
V — Voltage, volt
$\vec{v}$ — Absolute velocity vector, m/s
ω — Angular velocity, rad/s
w — Uncertainty
$\vec{w}$ — Relative velocity vector, m/s
Y_M — Contribution of the fluctuating dilatation
y^+ — Distance of the first cell center from the solid wall
z — Number of impeller blade
z_v — Number of diffuser blade
z_r — Number of diffuser return blade
η — The ratio between the time scales of the turbulence and the mean flow
η_e — Electric motor efficiency, %
η_h — Hydraulic efficiency, %
η_m — Mechanical efficiency, %
μ_t — Coefficient of turbulence dynamic viscosity, kg/m.s
σ_ε — Prandtl number for ε
σ_{ij} — Stress tensor
σ_k — Turbulent Prandtl number for k

∇ — Laplace operator
β_1 — Inlet blade angle of the impeller, ^{0}
β_2 — Outlet blade angle of the impeller, ^{0}
β_3 — Outlet blade angle of the diffuser, ^{0}
ε — Turbulence distribution rate
ε_k — Turbulent Prandtl number for ε
φ — Impeller wrap angle, ^{0}
φ_v — Diffuser wrap angle, ^{0}
φ_r — Diffuser return wrap angle, ^{0}
cosφ — Power factor
μ — Laminar dynamic viscosity coefficient, kg/m.s
ρ — density, kg/m^3
τ — Shear stress, kPa

References

[1] J. Perez, S. Chiva, W. Segala, R. Morales, C. Negrao, E. Julia, L. Hernandez, Performance Analysis of Flow in a Impeller-Diffuser Centrifugal Pumps Using CFD: Simulation and Experimental Data Comparisons, ECCOMAS CFD 2010, Lisbon, Portugal, 2010, pp. 1–18.
[2] M. Nataraj, R. Singh, Analyzing pump impeller for performance valuation using RSM and CFD, Desal. Wat. Treat., 52 (2014) 6822–6831.
[3] D. Kaya, E.A. Yagmur, K.S. Yigit, F.C. Kilic, A.S. Eren, C. Celik, Energy efficiency in pumps, Energy Convers. Manage., 49 (2008) 1662–1673.
[4] M.H. Aksoy, O. Babayigit, O. Kocaaslan, M. Ozgoren, Effect of Blade Wrap Angle to Centrifugal Pump Impeller Efficiency, Proc. International Conference: EFM 2013, Kutna Hora, Czech Republic, 2013, pp. 799–806.
[5] S. Chakraborty, K.M. Pandey, Numerical studies on effects of blade number variations on performance of centrifugal pumps at 4000 rpm, IJET, 3 (2011) 410–416.
[6] A. Arnone, P. Boncinelli, A. Munari, E. Spano, Application of CFD Techniques to the Design of the Ariane 5 Turbopump, 14th Computational Fluid Dynamics Conference, AIAA paper 99-3380, Norfolk, VA, USA, 1999, pp. 1087–1097.
[7] O. Babayigit, O. Kocaaslan, M.H. Aksoy, K.M. Güleren, M. Ozgoren, Numerical identification of blade exit angle effect on the performance for a multistage centrifugal pump impeller, EPJ Web Conf., 92 (2015) 1–7.
[8] S. Yedidiah, A study in the use of CFD in the design of centrifugal pumps, Eng. Appl. Comp. Fluid, 2 (2008) 331–343.
[9] M.L. Hedia, K. Hatema, Z. Ridhaa, Numerical analysis of the flow through in centrifugal pumps, Int. J. Therm. Technol., 2277–4114 (2012) 216–221.
[10] V. Godbole, R. Patil, S.S. Gavade, Axial Thrust in Centrifugal Pumps – Experimental Analysis, ICEM 15, Porto/Portugal, 2012, pp. 1–14.
[11] The Centrifugal Pump, Grundfos Research and Technology, Chapter 5, Pump Losses, Grundfos Management A/S, Bjerringbro, Denmark, 2012.
[12] J.F. Gulich, Centrifugal Pumps, Springer, Berlin, Germany, 2014.
[13] B. Cui, Z. Zhu, J. Zhang, Y. Chen, The flow simulation and experimental study of low-specific-speed high-speed complex centrifugal impellers, Chin. J. Chem. Eng., 14 (2006) 435–441.
[14] B. Jafarzadeh, A. Hajari, M.M. Alishahi, M.H. Akbari, The flow simulation of a low-specific-speed high-speed centrifugal pump, Appl. Math. Modell., 35 (2011) 242–249.
[15] W.G. Li, Effects of viscosity on turbine mode performance and flow of a low specific speed centrifugal pump, Appl. Math. Modell., 40 (2016) 904–926.
[16] K.W. Cheah, T.S. Lee, S.H. Winoto, Z.M. Zhao, Numerical flow simulation in a centrifugal pump at design and off-design conditions, Int. J. Rotating Mach., 2007 (2007) 1–8.
[17] H. Safikhani, A. Khalkhali, M. Farajpoor, Pareto based multi-objective optimization of centrifugal pumps using CFD, neural networks and genetic algorithms, Eng. Appl. Comp. Fluid, 5 (2011) 37–48.
[18] K.H. Wu, B.J. Lin, C.I. Hung, Novel design of centrifugal pump impellers using generated machining method and CFD, Eng. Appl. Comp. Fluid, 2 (2008) 195–207.
[19] O. Kocaaslan, M.H. Aksoy, O. Babayigit, M. Ozgoren, An Experimental Investigation of Surface Roughness Influence on Centrifugal Pump Characteristics, Proc. International Conference: EFM 2013, Kutna Hora, Czech Republic, 2013, pp. 814–819.
[20] W. Jiang, G. Li, P.F. Liu, L. Fu, Numerical investigation of influence of the clocking effect on the unsteady pressure fluctuations and radial forces in the centrifugal pump with vaned diffuser, Int. Commun. Heat Mass Transfer, 71 (2016) 164–171.
[21] H. Stel, T. Sirino, F.J. Ponce, S. Chiva, R.E.M. Morales, Numerical investigation of the flow in a multistage electric submersible pump, J. Pet. Sci. Eng., 136 (2015) 41–54.
[22] F. Ayad, H.M. Abdalla, A. Abou El-Azm Aly, Effect of semi-open impeller side clearance on the centrifugal pump performance using CFD, Aerosp. Sci. Technol., 47 (2015) 247–255.
[23] A. Engeda, M. Rautenberg, Partial Flow Performance Comparisons of Semi-open and Closed Centrifugal Impellers, ImechE, C334/88 Edinburgh, U.K. Bury St. Edmunds, U.K., Mech. Engng. Publications Ltd., 1988.
[24] S. Liu, N. Michihiro, K. Yoshida, Impeller geometry suitable for mini turbo-pump, J. Fluids Eng., 123 (2001) 500–506.
[25] H. Liu, J. Wang, Y. Wang, H. Huang, L. Jiang, Partially-averaged Navier-Stokes model for predicting cavitating flow in centrifugal pump, Eng. Appl. Comp. Fluid, 8 (2014) 319–329.
[26] L. Zhou, W. Shi, W. Lu, B. Hu, S. Wu, Numerical investigations and performance experiments of a deep-well centrifugal pump with different diffusers, J. Fluids Eng., 134 (2012) 1–8.
[27] S.D. Kyparissis, E.C. Douvi, E.E. Panagiotopoulos, D.P. Margaris, A.E. Filios, CFD flow field analysis and hydrodynamic double-arc blade design effects for optimum centrifugal pump performance, Int. Rev. Mech. Eng., 3 (2009) 284–294.
[28] Anonymous, Fluent 14.0 User Guide, Fluent Inc., 2015.
[29] H. Versteeg, W. Malalasekra, An Introduction to Computational Fluid Dynamics: The Finite Volume Method, John Wiley & Sons, New York, 1995.
[30] K.M. Pandey, S. Chakraborty, A.P. Singh, Numerical analysis of centrifugal pumps with fluent software, Int. J. Appl. Eng. Res., 6 (2011) 1117–1126.
[31] W.B. Fan, W.G. Li, X.J. Gong, X.R. Zhang, Evaluation of the effect of a hydraulic impeller in a flocculation basin on hydrodynamic behavior using computational fluid dynamics, Desal. Wat. Treat., 54 (2015) 1361–1374.
[32] K.K. Singh, S.M. Mahajani, K.T. Shenoy, A.W. Patwardhan, S.K. Ghosh, CFD modeling of pilot-scale pump-mixer: single-phase head and power characteristics, Chem. Eng. Sci., 62 (2007) 1308–1322.
[33] B.K. Baysal, Centrifugal Pumps Account Drawings and Construction Specifications, Istanbul Technical University Publishing House, 1979. (in Turkish)
[34] J.P. Holman, J.G. Walter, Experimental Methods for Engineers, 2nd ed., McGraw-Hill, New York, 1994.
[35] O. Kocaaslan, M. Ozgoren, M.H. Aksoy, O. Babayigit, Experimental and numerical investigation of coating effect on pump impeller and volute, J. Appl. Fluid Mech., 9 (2016) 2475–2487.
[36] S.S. Yang, S. Derakshan, F.Y. Kong, Theoretical, numerical and experimental prediction of pump as turbine performance, Renew. Energy, 48 (2012) 507–513.
[37] S. Salvodori, A. Marini, F. Martelli, Methodology for the residual axial thrust evaluation in multistage centrifugal pumps, Eng. Appl. Comp. Fluid, 6 (2012) 271–284.
[38] P. Adami, S.D. Gatta, F. Martelli, L. Bertolazzi, D. Maestri, G. Marenco, A. Piva, Multistage Centrifugal-Pumps: Assessment of a Mixing Plane Method for CFD Analysis, 60° Congresso Nazionale ATI, Rome, 2005.